Raman-scattering study of isotopically engineered crystalline C_{60}

P. J. Horoyski and M. L. W. Thewalt
Department of Physics, Simon Fraser University, Burnaby, British Columbia, Canada V5A 1S6

T. R. Anthony
GE Corporation Research & Development Center, General Electric Company, Schenectady, New York 12301

(Received 10 January 1996)

A high resolution Raman scattering study of the intramolecular phonons of crystalline C_{60} is presented. Many of the Raman-active vibrations are richly structured, revealing a crystal field splitting both above and below the orientational ordering transition at 260 K. Much of the vibrational fine structure is also shown to be strongly influenced by the small amount of orientational, or merohedral, disorder which persists in the low-temperature phase. The impact of isotopic disorder is examined by the comparison of Raman spectra of single crystals made from naturally abundant carbon, 99.95% ^{12}C, and 99.7% ^{13}C, as well as a range of intermediate ^{13}C concentrations. The $^{12}C_{60}$ and $^{13}C_{60}$ spectra are identical, apart from a uniform softening of the $^{13}C_{60}$ vibrational energies by the factor $(\frac{12}{13})^{1/2}$. As the ^{13}C concentration is increased from approximately zero, the bulk of the vibrational modes display only a softening in energy and a broadening in width. In sharp contrast to this expected behavior is the $A_g(2)$-derived band which shows both a softening in energy and additional splittings with increasing ^{13}C content. [S0163-1829(96)05218-6]

INTRODUCTION

The study of vibrational modes in crystalline C_{60} has attracted considerable theoretical[1–6] and experimental[7–18] interest for the past several years. Crystalline C_{60} is a prototypical molecular solid; the intramolecular bonding is much stronger than the intermolecular bonding, allowing the phonons of the crystal to be divided into several distinct types. The phonon spectrum contains high energy modes in the range of $\sim$260–1600 cm^{-1}, phonons which originate from vibrations within the molecular units of the crystal. The spectrum of these intramolecular phonons coarsely mirrors the vibrational spectrum of an isolated molecule, although many optically silent vibrations of the isolated molecule are active in the crystal,[14,15] and some splittings of the degenerate molecular vibrations have been reported for the solid.[11,13,17] Having no counterpart in an isolated molecule are the low-energy ($\sim$20–60 cm^{-1}) lattice modes of the solid which consist of translational motions of the rigid molecular units (intermolecular phonons) and librational excitations of the molecules (librons). The intermolecular phonons and librons are visible at temperatures below 260 K, the order-disorder phase transition temperature of the solid. At room temperature, the C_{60} molecules undergo isotropic rotation[19] while positioned at face centered cubic (fcc) lattice sites,[20] but upon cooling below 260 K, the molecules assume preferred orientations, forming a simple cubic (sc) structure with four molecules per unit cell.[21]

While long range orientational order exists in the crystal below 260 K, a significant fraction of the molecules remain misoriented. This orientational, or merohedral,[22] disorder is reduced as the temperature is lowered to $\sim$90 K, below which a second, ''glassy'' transition freezes in a small amount of static disorder.[22] Surprisingly, this orientational disorder has recently been shown to lead to a splitting of some of the intramolecular vibrations which otherwise show no splitting due to the static crystal field.[17]

Another form of disorder arises from isotopic substitutions of ^{13}C for ^{12}C within the molecules. The 1.1% natural abundance of ^{13}C implies that nearly half of the molecules in solid C_{60} contain at least one ^{13}C atom. In a ''conventional'' crystal such as diamond, the phonons sample a large number of unit cells, leading to a linear averaging of the isotopic masses. In this case, the isotopic disorder simply leads to a shift of the phonon frequencies by $\overline{m}^{-(1/2)}$, where $\overline{m}$ is the average atomic mass, along with a broadening of the phonon linewidths due to the mass fluctuations.[23] A more complicated dependence upon isotopic content could be expected from the intramolecular phonons of solid C_{60} given the molecular origin of the modes. A Raman-scattering study[17] of natural and ^{12}C enriched C_{60} has in fact shown that dramatic isotopic-disorder induced changes occur within the $A_g(2)$-derived phonon band; in addition to energy shifts, very pronounced splittings were seen from $^{12}C_{60}$ to natural C_{60}.

In this work we present a high resolution Raman-scattering study of the intramolecular phonon spectrum of crystalline C_{60}. Fine structure is evident in most of the Raman-active molecular modes, as well as in two intramolecular modes which are seen in the solid state but are optically silent in an isolated molecule. The small splittings of the phonons are resolvable due to the narrow vibrational linewidths seen in good quality single crystals. The bulk of the observed splittings are determined not to arise from isotopic substitutions by comparing spectra of crystalline C_{60} made from naturally abundant, 99.95% ^{12}C, and 99.7% ^{13}C carbon. Several modes do show slightly reduced linewidths in the $^{12}C_{60}$ enriched samples, while other modes show virtually no change from the naturally abundant material to the ''pure'' $^{12}C_{60}$ material [a straightforward $(\frac{12}{13})^{1/2}$ energy softening is, however, seen between $^{12}C_{60}$ and $^{13}C_{60}$ for the entire phonon spectrum]. Splittings due to isotopic disorder

were only observed in the $A_g(2)$ band and the silent mode attributed to $F_{2g}(1)$. As we have previously reported, $A_g(2)$ displays an unexpected dependence upon the isotopic composition of the crystal, showing a splitting which is not simply related to the differences seen for isolated molecules in solution.[17,24] Motivated by this unexplained behavior of $A_g(2)$ with isotopic disorder, we have produced and studied C_{60} crystals with ^{13}C concentrations of 0.5%, 7.3%, and 56.1%. The 0.5% ^{13}C sample is only a small departure from natural abundance, but substantial changes within the $A_g(2)$ band are observed. In the 7.3% ^{13}C material, the $A_g(2)$ band broadens considerably, but additional splittings are resolvable, while in the 56.1% ^{13}C crystal, fine structure can no longer be resolved in the broadened $A_g(2)$ band.

Since the majority of the observed Raman fine structure does not stem from isotopic disorder, it can be assigned to the crystal field. However, a significant component of the crystal field splittings observed in the low temperature phase is seen to arise from merohedral disorder. The small fraction of misoriented molecules within the ordered crystal influences the energies and intensities of most of the Raman-active vibrational fine structure.

EXPERIMENT

The samples used in this study were prepared from commercially available C_{60} powder (Texas Fullerenes, Hoechst), as well as C_{60} powder produced in-house using a carbon arc discharge.[25] Isotopically enriched C_{60} powder was made using graphite rods grown pyrolytically from isotopically enriched methane gas (Cambridge Isotope Labs). C_{60} powder composed of naturally abundant carbon was also made using this technique; no difference in the Raman spectra of crystals made from it and the commercially available powder was observed. Large (several >10 mm^3), highly faceted single crystals were grown by sublimation of the C_{60} powder in a temperature gradient under vacuum, after outgassing the powder at 250 °C under vacuum. The resultant crystals were further purified by multiple vacuum regrowths.

The Raman spectra were collected using either a Bomem DA8.01 interferometer or a single stage grating spectrometer and cooled CCD detector. The maximum interferometer resolution used was 0.025 cm^{-1}, while the dispersive spectrometer had an instrumental resolution of 0.3 cm^{-1} at 895 nm. The excitation source was a Ti:sapphire laser which was line narrowed and frequency stabilized by means of an intracavity etalon. Rejection of elastically scattered laser light was achieved by means of an atomic vapor (cesium or rubidium) filter.[26] All of the Raman fine structure presented was independent of the excitation intensity (10–100 mW) and wavelength (794.98 and 894.60 nm) used. The use of such longer wavelength excitation leads to large Raman signals due to the transparency of the samples, and also eliminates problems related to sample heating and photodegradation.[9]

RESULTS AND DISCUSSION

The low-temperature Raman spectrum of crystalline C_{60} made from naturally abundant carbon (henceforth referred to as ''natural C_{60}'') is shown in Fig. 1. The absence of a broad

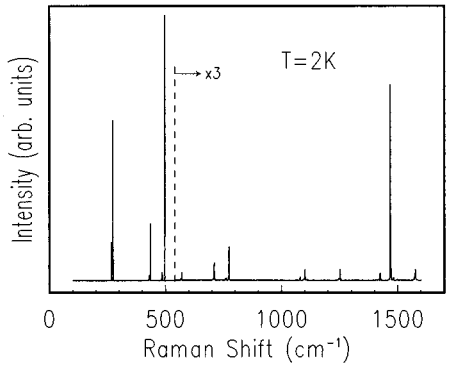

FIG. 1. Unpolarized Raman spectrum of a C_{60} single crystal at 2 K (895 nm excitation and 0.10 cm^{-1} resolution). The higher energy portion of the spectrum (>600 cm^{-1} shift) has been scaled up in intensity by a factor of 3 for clarity.

fluorescence background which is typically seen underlying Raman spectra of C_{60} stems from using near-infrared excitation rather than visible wavelengths, to which the material is opaque. The relative intensities of the modes also differ from that of previously reported Raman spectra collected using visible excitation. This arises from a resonant enhancement of several modes with short wavelength pumping,[10] the ω^4 dependence of the Raman cross-section suppressing the higher energy modes more in the near-infrared than in the visible, and the coarser resolutions previously used[11,13] producing reduced peak intensities for the narrower modes relative to the intrinsically broader modes. As can be seen in Fig. 1, more than simply ten H_g and two A_g molecular modes are visible in Raman scattering from the crystal, while splittings of several modes has occurred, most notably in the lowest energy $H_g(1)$-derived mode.

The intramolecular phonon spectrum, along with its temperature evolution, is shown in an expanded energy scale in Fig. 2 (the weak combination bands previously studied by others[14,15] are not under consideration in this work). As is clearly evident in Fig. 2, nearly all of the Raman modes display complex fine-structure at low temperature. While the splittings in many cases are small, the narrow linewidths of the modes make the structure resolvable. $H_g(1)$, the lowest-energy intramolecular phonon, is clearly a doublet in the high temperature fcc phase, while in the low-temperature (<260 K) orientationally ordered phase it appears as a quartet. Since $H_g(1)$ is well separated in energy from the nearest silent mode,[4,14,15] and since difference scattering can be neglected at the lowest temperatures, all of these components can be attributed with certainty to $H_g(1)$. As was earlier noted,[17] the observed low-temperature splitting is in fact in good agreement with a recent band structure calculation.[4]

Next in Fig. 2 is shown the $H_g(2)$ derived band. As was the case with $H_g(1)$, $H_g(2)$ is well isolated in energy from neighboring silent modes and possible overtones, and so all of the structure arises from splittings of the $H_g(2)$ mode. In the high-temperature (HT) phase, a doublet is resolvable. Upon cooling into the low-temperature (LT) phase, the linewidths narrow considerably and the band becomes richly structured. The highest energy component of $H_g(2)$ possesses one of the narrowest linewidths seen in the entire spectrum, measuring 0.10 cm^{-1} at 2 K.

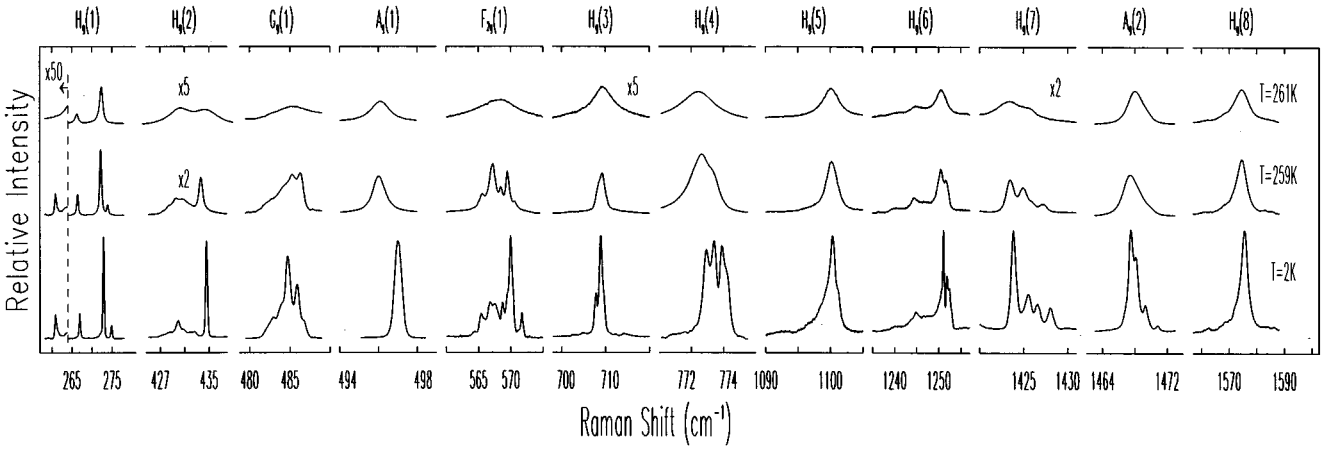

FIG. 2. The temperature evolution of the $H_g(1)$, $H_g(2)$, $G_g(1)$, $A_g(1)$, $F_{2g}(1)$, $H_g(3)$, $H_g(4)$, $H_g(5)$, $H_g(6)$, $H_g(7)$, $A_g(2)$, and $H_g(8)$ Raman components (from left to right) of crystalline C_{60}. The spectra within each subsection of the energy axis are plotted on the same scale, but shifted for clarity.

Following the $H_g(2)$ band in Fig. 2 is seen a mode ascribed[14] to $G_g(1)$. While this vibration is silent in the isolated molecule, it and all the gerade vibrations are symmetry allowed in the crystal state.[3] In the HT phase, only a single broad band is observed, while in the LT phase the integrated intensity increases, the linewidths narrow, and at least five components become resolvable. This behavior is mirrored in the $F_{2g}(1)$ mode,[14] seen in Fig. 2 centered at $\sim$570 cm^{-1}. This silent mode also appears in the HT crystal as a single broad band while many components are visible in the LT phase. None of the fine structure present in either the $G_g(1)$ or $F_{2g}(1)$ bands corresponds to other nearby silent modes or overtone scattering, and so can be solely attributed to these two molecular modes.

In contrast to all of the phonon bands discussed so far, the $A_g(1)$-derived phonon at $\sim$497 cm^{-1} is a single, unsplit peak in both the HT and LT phases. As can be seen in Fig. 2, $A_g(1)$ narrows and shifts to slightly higher energy as the temperature is lowered through the ordering transition, but no fine structure develops in the LT phase.

The $H_g(3)$ mode, centered at $\sim$710 cm^{-1}, and the $H_g(5)$ mode at $\sim$1100 cm^{-1} both appear as a single broad band in the freely rotating HT phase, but upon cooling into the orientationally ordered LT phase, the linewidths narrow sufficiently to resolve small splittings of the main peaks. The assignment of all the observed structure centered at 710 and 1100 cm^{-1} to $H_g(3)$ and $H_g(5)$, respectively, is complicated by the presence of several sum modes within $\sim$5 cm^{-1} of these two fundamentals.[4,14,15] The weak feature just below $H_g(3)$ at 706 cm^{-1} coincides in energy with $H_g(1)+H_g(2)$, while its small integrated intensity relative to the main peak of $H_g(3)$ corroborates its identification as an overtone mode.

The $H_g(4)$ derived phonon band, centered at $\sim$774 cm^{-1} in Fig. 2, shows no structure beyond an asymmetric line shape in the HT phase, but at low temperatures, four nearly equal intensity components are clearly present. $H_g(4)$ also has several nearby combination mode possibilities (the higher in energy one goes, the more likely this becomes). However, the four components seen in Fig. 2 all have a strong Raman signal and so can be attributed to $H_g(4)$, since combination mode scattering is expected to be much weaker than scattering from the allowed fundamental modes. The lower energy foot at $\sim$771 cm^{-1} coincides in energy with $H_g(1)+A_g(1)$, and so likely stems from this combination mode scattering.

Structure is visible both above and below the ordering transition for the $H_g(6)$ and $H_g(7)$ bands centered at 1250 and 1425 cm^{-1}, respectively. At low temperature, $H_g(7)$ consists of a fundamental peak with three distinct, higher energy components, while $H_g(6)$ displays a complex combination of several sharp components and broad, unresolved background scattering. Like $H_g(7)$, the second A_g mode at $\sim$1468 cm^{-1} also displays a series of resolved components at low temperature, but only an asymmetry in the line shape remains in the freely rotating HT phase.

Finally, the highest energy first-order mode, $H_g(8)$, is also the intrinsically broadest band. Even at the lowest temperatures, no fine structure is visible, although the low-energy asymmetry of the band does suggest an unresolved splitting. As the temperature is raised the mode softens, and as was the case for all the Raman modes, the integrated intensity decreases.

The polarization dependence of the phonon bands which display resolvable splittings is shown in Fig. 3. As noted earlier, solid C_{60} was transparent to the near-infrared wavelength excitation employed in this work. This presented an unforseen difficulty to the polarization measurements due to the morphology of the crystals. The samples were highly faceted with smooth, shiny faces, except for the portion of the crystal which was surface roughened due to contact with the quartz growth tube. The morphology of the crystals was such that no crystal face could be excited with the laser beam without having the beam exit the crystal through the roughened side. The laser excitation was diffusely scattered by the roughened face, so that the emerging laser light retained very little of its initial polarization. The high index of refraction of solid C_{60} caused the diffusely scattered laser light (and the Raman signal) to undergo multiple reflections within the crystal before being collected by the spectrometer, thereby scrambling the polarization state of the Raman modes. By

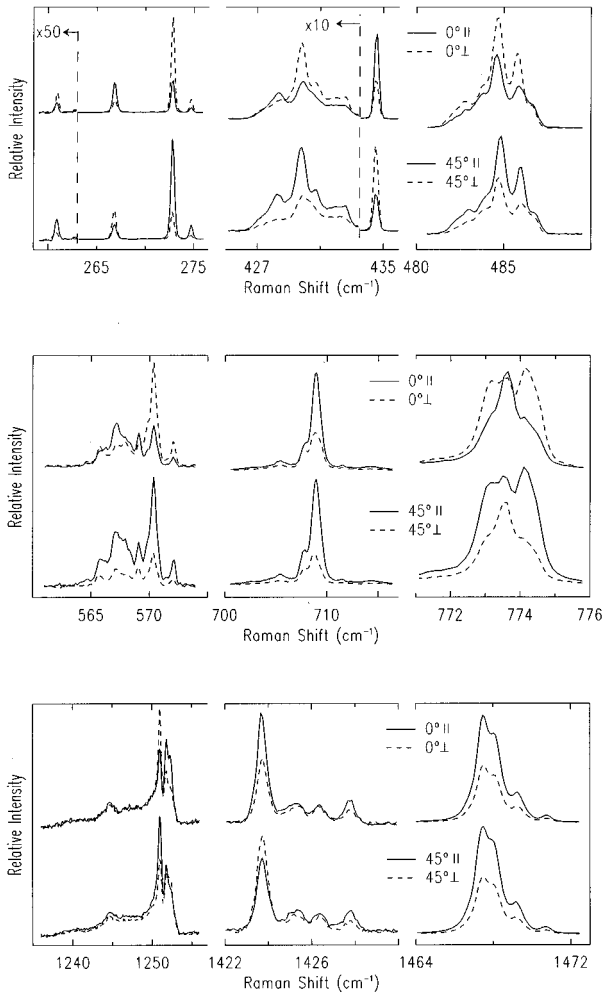

FIG. 3. Polarization dependence of the Raman-active phonons of crystalline C_{60} which display resolvable fine structure. The measurements were made from a {100} face of the crystal in a backscattering geometry; $T=2$ K. 0° and 45° refer to the angle of the laser polarization relative to the [001] direction while ∥ and ⊥ refer to the relative orientation of the incident and scattered light polarizations.

mechanically and chemically polishing the face through which the laser beam exited, the amount of diffusely scattered light was greatly reduced. Nonetheless, if all of the Raman signal generated within the sample was collected, the degree of polarization of the Raman modes remained quite poor. By employing a two-dimensional focal plane array detector with the dispersive spectrometer, Raman scattering was seen to arise not only from the area of the laser spot, but from the entire height of the sample. If only the Raman signal originating directly from the laser spot was accepted, a marked improvement in the polarization of the scattered light was seen. Under these conditions, the $A_g(1)$ mode had a depolarization ratio ρ ($\rho=I_\perp/I_\parallel$) of 0.25. While this is an order of magnitude larger than the value typically seen using visible excitation (which because of its short penetration length in C_{60} does not suffer from these polarization scrambling effects), it is sufficient to allow a symmetry identification of the fine-structure components of the phonon modes.

The measurements depicted in Fig. 3 were made from a {100} face of the crystal in a backscattering geometry. In Fig. 3, 0° and 45° refer to the setting angle of the laser polarization relative to ⟨001⟩, while ∥ and ⊥ refer to the relative orientation of the incident and scattered light polarization. The factor-group analysis for the LT phase has been previously determined,[3] and is reproduced (for the gerade modes) in Table I. The components which are expected to appear in the various scattering geometries employed in this work are listed in Table II. The splittings of $H_g(3)$ and $H_g(4)$ are not fully resolved in Fig. 3 due to the lower resolution of the grating spectrometer as compared to the interferometer.

TABLE I. Correlation table of the gerade modes of C_{60} for the low temperature phase of solid C_{60}. Only the ten H_g and two A_g modes are Raman active in the isolated molecule, while all gerade modes are allowed by symmetry in the solid phase (LT and HT) (Ref. 3).

Molecule I_h	LT phase (sc) T_h^6
$2A_g$	$2A_g+2F_g$
$3F_{1g}$	$3A_g+3E_g+9F_g$
$4F_{2g}$	$4A_g+4E_g+12F_g$
$6G_g$	$12A_g+6E_g+24F_g$
$8H_g$	$8A_g+16E_g+40F_g$

The enumeration and symmetry identification of the fine-structure components of many of the modes shown in Fig. 3 can in principle be accounted for solely by crystal field splittings of the degenerate molecular vibrations. A recent theoretical lattice dynamics study[4] has in fact predicted that most of the Raman active phonons show strong dispersions, particularly those below $\sim 600\ \mathrm{cm}^{-1}$. The T_h^6 space group of the low temperature phase cannot, however, account for the polarization dependence of the $A_g(2)$-derived phonon band. The four resolvable components of $A_g(2)$ shown in Fig. 3 all exhibit an A_g-like polarization dependence, in sharp contrast to the expectations based on group-theory as summarized in Tables I and II. The bulk of the splittings of $A_g(2)$ have been previously shown[17] to stem from the mass defects (^{13}C substitutions) present in natural C_{60}, a perturbation which is neglected in the group-theory treatment presented here.

To eliminate the influence of this isotopic disorder, C_{60} single crystals with an enriched isotopic purity have been fabricated and studied. Using 99.95% ^{12}C starting material, crystals which are 97.3% $^{12}C_{60}$ have been made. $^{13}C_{60}$ crystals have also been made; a starting ^{13}C purity of 99.7%

TABLE II. Raman-active modes of solid C_{60} under various scattering geometries. The setting angle ϕ refers to the angle of the incident light polarization relative to the [100] crystal direction while ∥ and ⊥ refer to the relative orientation of the incident and scattered light polarization.

Setting angle ϕ	Analyzer	Backscattering from {100} face
0°	∥	A_g+E_g
	⊥	F_g
45°	∥	$A_g+E_g+F_g$
	⊥	E_g

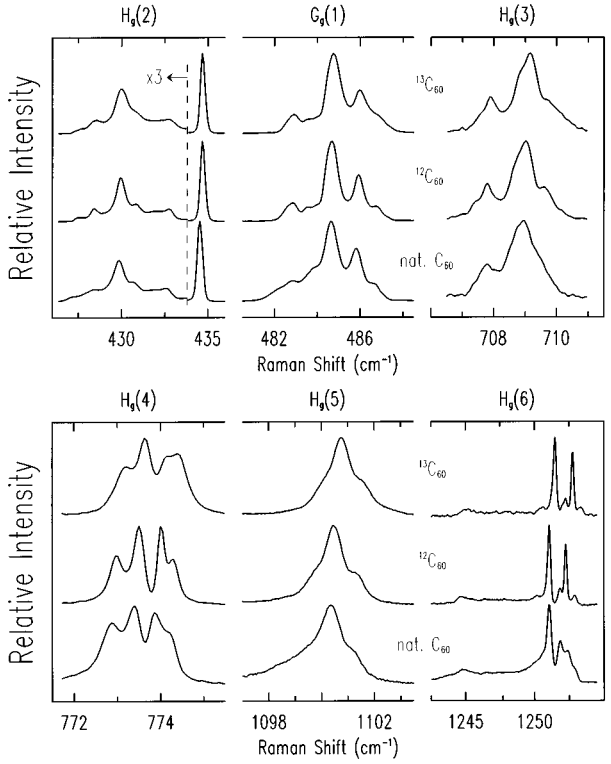

FIG. 4. $H_g(2)$, $G_g(1)$, $H_g(3)$, $H_g(4)$, $H_g(5)$, and $H_g(6)$ fine structure of crystalline C_{60} made from naturally abundant carbon, 99.95% ^{12}C, and 99.7% ^{13}C; $T=2$ K. The $^{13}C_{60}$ spectra have been scaled up in energy by the factor $(\frac{13}{12})^{1/2}$ to facilitate comparison.

produced crystals which were 85% pure $^{13}C_{60}$. For simplicity, the 97.3% $^{12}C_{60}$ crystals and 85% $^{13}C_{60}$ crystals will be herein referred to as ''crystalline $^{12}C_{60}$'' and ''crystalline $^{13}C_{60}$,'' respectively. In Fig. 4, subsets of the low temperature Raman spectra of natural C_{60}, $^{12}C_{60}$, and $^{13}C_{60}$ crystals are shown. The natural C_{60} and $^{12}C_{60}$ spectra are shown on the same energy scale, while the $^{13}C_{60}$ spectra have been scaled up in energy by the factor $(\frac{13}{12})^{1/2}$ to facilitate comparison. All of the modes shown in Fig. 4 display narrower linewidths in the isotopically purified materials as compared to natural C_{60}, but none of the fine structure is absent. The random substitutions of ^{13}C for ^{12}C present in natural C_{60} are thus not responsible for the splittings seen in these modes. The line broadening due to random isotopic substitutions in natural C_{60} is evident in all of the modes shown in Fig. 4, but is most notable for $H_g(6)$, where additional components can be resolved in the $^{12}C_{60}$ and $^{13}C_{60}$ spectra, and the broad background scattering is reduced.

Linewidth broadening arising from isotopic disorder does not occur in all of the intramolecular phonons. Shown in Fig. 5 are several modes which display little or no broadening in natural C_{60} relative to the isotopically purified samples. The $^{13}C_{60}$ spectra shown in Fig. 5 have been scaled up in energy by the factor $(\frac{13}{12})^{1/2}$ as was done in Fig. 4. Immediately obvious from Fig. 5 is the fact that the phonon fine structure is unchanged from natural C_{60} to the isotopically purified $^{12}C_{60}$ and $^{13}C_{60}$. Like the modes shown in Fig. 4 then, all of the splittings arise from crystal field effects rather than isotopic disorder.

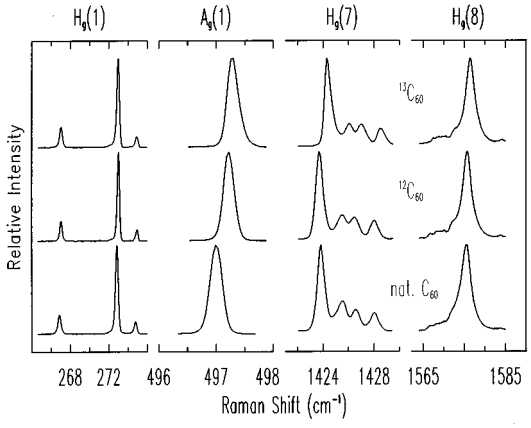

FIG. 5. $H_g(1)$, $A_g(1)$, $H_g(7)$, and $H_g(8)$ fine structure of crystalline C_{60} made from naturally abundant carbon, 99.95% ^{12}C, and 99.7% ^{13}C; $T=2$ K. The $^{13}C_{60}$ spectra have been scaled up in energy by the factor $(\frac{13}{12})^{1/2}$ for ease of comparison.

Isotopic disorder does lead to activation of additional fine structure rather than simply shifting components in two intramolecular modes; $F_{2g}(1)$ and $A_g(2)$, shown in Fig. 6. While $F_{2g}(1)$ is a complex band in natural C_{60} and the isotopically purified $^{12}C_{60}$ and ^{13}C samples, the component at 569.39 cm^{-1} is clearly present in only natural C_{60}. The isotope dependence of $A_g(2)$ is the most pronounced of all the Raman modes. In natural C_{60}, $A_g(2)$ has at least five components at 1466.9, 1467.6, 1468.2, 1469.4, and 1470.8 cm^{-1}, while in $^{12}C_{60}$, only peaks at 1468.6 and 1470.8 cm^{-1} are visible. Thus the $A_g(2)$ band appears more molecular in nature than the other C_{60} phonons, in that the isotopic disorder is not averaged over. However, the splittings displayed in Fig. 6 cannot be understood within a purely molecular description of the vibrational mode. It was shown in Raman-scattering studies of isolated C_{60} molecules (frozen solutions of C_{60} in CS_2) that the isotopes of naturally abundant carbon led to fine structure within the $A_g(2)$ molecular vibration. This fine structure stemmed from a simple superposition of peaks corresponding to $^{12}C_{60}$, $^{13}C^{12}C_{59}$, and $^{13}C_2{}^{12}C_{58}$

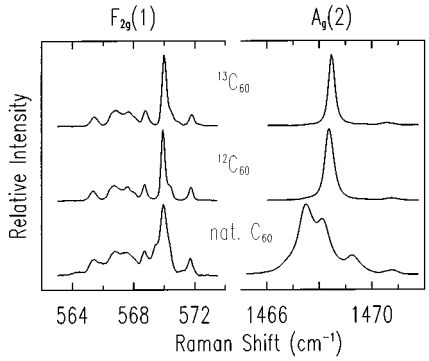

FIG. 6. $F_{2g}(1)$ and $A_g(2)$ fine structure of crystalline C_{60} made from naturally abundant carbon, 99.95% ^{12}C, and 99.7% ^{13}C; $T=2$ K. The $^{13}C_{60}$ spectra have been scaled up in energy by the factor $(\frac{13}{12})^{1/2}$ to facilitate comparison. The $F_{2g}(1)$ and $A_g(2)$ modes are the only two phonons in the first-order Raman spectrum which display additional splittings due to isotopic disorder.

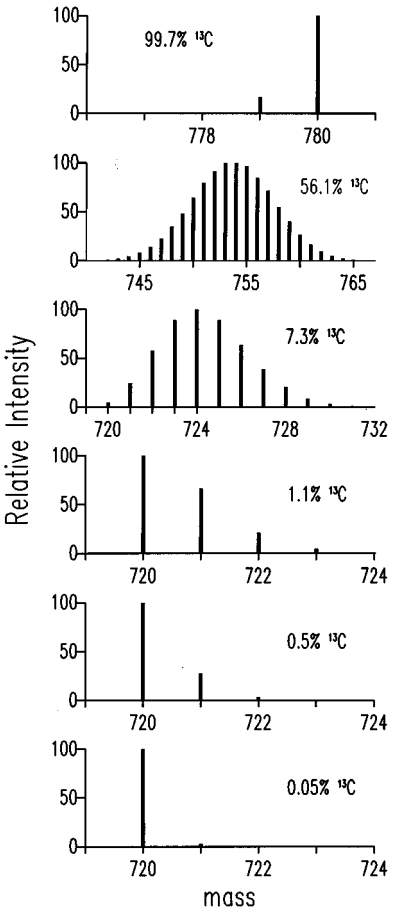

FIG. 7. The measured mass abundances of C_{60} molecules made from isotopically enriched graphite rods and rods made from naturally abundant carbon (1.1% ^{13}C).

vibrations.[17,24] This is clearly not the case in the solid state; none of the components of the $A_g(2)$ phonon in natural crystalline C_{60} are degenerate with the strongest peak in crystalline $^{12}C_{60}$, despite the fact that over half of the molecules present in natural C_{60} are $^{12}C_{60}$. The energies of all the Raman modes discussed in this and the preceding section are summarized in Table III.

The range of responses of the intramolecular phonons to isotopic disorder can be qualitatively understood by expressing the relative mass fluctuations as a frequency bandwidth, $(\Delta m/\overline{m})\omega_0$, and comparing it with the bandwidth, $\Delta\omega_0$, of the intramolecular phonons in the first Brillouin zone. If the mass fluctuation bandwidth is much smaller than the intrinsic phonon bandwidth, one would anticipate a simple linear averaging of the isotope masses to result, as is seen in ''conventional'' semiconductors such as germanium.[27] A more complicated behavior could be expected when the mass fluctuation bandwidth becomes comparable in magnitude to the intrinsic phonon bandwidth. For the lower-energy intramolecular phonons, significant band dispersions have been predicted[4] while the mass-fluctuation bandwidth is smallest, and so one would expect little response from these modes to increasing ^{13}C content beyond a uniform softening. The 0.11 cm^{-1} shift of $H_g(1)$, 0.15 cm^{-1} shift of $H_g(2)$, and 0.20 cm^{-1} shift of $A_g(1)$ observed between natural C_{60} and $^{12}C_{60}$

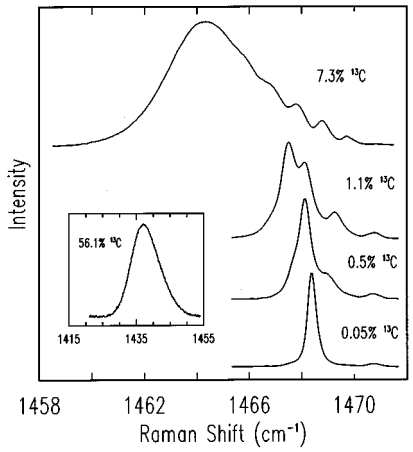

FIG. 8. $A_g(2)$-derived phonon band of crystalline C_{60} as a function of isotope content; $T=2$ K.

are, in fact, exactly what one would expect using a $\overline{m}^{-(1/2)}$ dependence of the phonon frequencies, where $\overline{m}$ is the average isotope mass. Conversely, the $A_g(2)$ mode is predicted to have a negligibly small phonon bandwidth[4] while the isotopic-disorder bandwidth, which scales with the mode frequency, is significantly larger than it was for the lower-energy phonons. A complicated interplay between solid state and isotope effects is therefore seen within the $A_g(2)$-derived phonon.

To further explore the complex dependence of $A_g(2)$ on the isotopic composition of the crystal, additional samples with varying mass compositions have been fabricated. Figure 7 shows the mass spectra of the isotopically engineered crystals used in this study. As can be seen in Fig. 7, natural C_{60} contains significant amounts of $^{13}C^{12}C_{59}$ and $^{13}C_2{}^{12}C_{58}$. By using a starting ^{13}C content of 0.50%, roughly half that of the natural material (1.1% ^{13}C), C_{60} molecules with one and two ^{13}C atoms are still produced but in reduced concentrations. This then provides a convenient isotopic composition between natural C_{60} and the ''pure'' $^{12}C_{60}$ material. By increasing the ^{13}C concentration to 7.3%, the number of different molecular masses present is greatly increased, and the most abundant species is no longer the pure $^{12}C_{60}$ molecule. At 56.1% ^{13}C concentration, the isotopic disorder of the crystal is nearly maximized, both in the number of different molecular masses present, and in the number of possible isomers with a fixed molecular mass.

The $A_g(2)$ band of crystalline C_{60} as a function of isotopic composition is shown in Fig. 8. While the mass spectrum of the 0.50% ^{13}C material represents only a small departure from that of natural C_{60}, substantial changes have occurred within $A_g(2)$. Only four components are visible in the 0.50% ^{13}C material, at 1467.7, 1468.1, 1469.0, and 1470.8 cm^{-1}. The highest energy component at 1470.8 cm^{-1} is unchanged as the ^{13}C content is increased from the $^{12}C_{60}$ sample to natural C_{60}; the correlation between the remaining components is somewhat ambiguous, however. One possibility has the four components of natural C_{60} at 1466.9, 1467.7, 1468.2, and 1469.4 cm^{-1} collapsing from both higher and lower energy to the single peak seen in crystalline $^{12}C_{60}$ at 1468.6 cm^{-1}. Alternatively, the main peak of crystalline $^{12}C_{60}$ may be softening with increasing ^{13}C content according

TABLE III. Phonon mode energies.

265 K (fcc) natural C_{60}	2 K (sc) natural C_{60}	2 K $^{12}C_{60}$	2 K $^{13}C_{60}$	Assignment
	260.96	260.13	251.03	
266.2	266.87	266.98	256.61	
272.4	272.83	272.94	262.31	$H_g(1)$
	274.76	274.89	264.17	
	427.19	427.66	410.88	
	428.32	428.40	411.80	
	429.82	429.96	413.24	
430.3	430.72	430.88	414.11	$H_g(2)$
	431.61	431.90	415.15	
	432.59	432.77	415.95	
434.3	434.54	434.69	417.84	
	482.79	482.79	464.10	
	483.79	483.59	465.17	
485.4	484.67	484.69	465.86	$G_g(1)$
	485.80	485.91	467.11	
	486.67	486.77	467.94	
496.1	497.00	497.22	477.89	$A_g(1)$
	565.52	565.35	543.35	
	566.73	566.71	544.69	
567.8	567.52	567.58	545.42	
	568.77	568.71	546.60	$F_{2g}(1)$
	569.39			
	569.94	569.92	547.75	
	570.36	570.34	548.20	
	571.70	571.75	549.51	
	707.46	707.40	679.95	
	707.81	707.79	680.28	
709.4	708.58	708.69	681.19	$H_g(3)$
	709.01	709.09	681.48	
	709.57	709.63	682.04	
	772.88	772.99	743.04	
772.4	773.41	773.50	743.46	$H_g(4)$
	773.87	774.01	743.96	
	774.23	774.30	744.19	
		1099.70	1057.33	
1100.0	1100.36	1100.50	1057.89	$H_g(5)$
	1101.38	1101.37	1058.67	
	1244.84	1244.85	1196.48	
1244.9		1250.18	1201.79	
	1251.08	1251.07	1202.65	$H_g(6)$
1250.5	1251.86	1251.86	1203.39	
	1252.41	1252.27	1203.88	
	1252.88	1252.86	1204.45	
	1423.80	1423.72	1368.82	
1423.4	1425.52	1425.51	1370.39	$H_g(7)$
	1426.57	1426.49	1371.48	
1425.5	1427.90	1427.92	1372.84	
	1466.9			
	1467.6			
1468.1	1468.8	1468.6	1412.00	$A_g(2)$
	1469.4			
	1470.8	1470.8	1414.00	
	1572.22	1572.32	1511.80	$H_g(8)$
1574.5	1575.51	1575.68	1514.95	

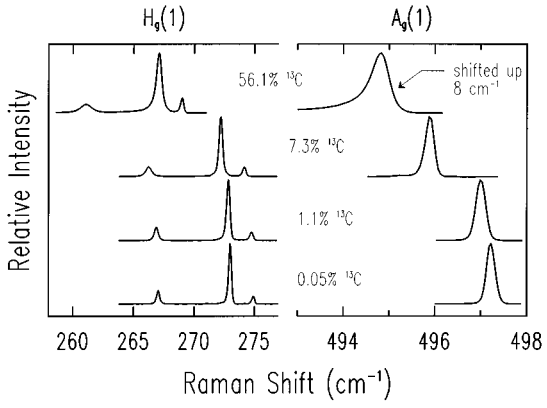

FIG. 9. $H_g(1)$ and $A_g(1)$ modes of crystalline C_{60} as a function of isotope content; $T=2$ K. The $A_g(1)$ spectrum of the 56.1% ^{13}C C_{60} crystal has been shifted upward in energy by 8 cm^{-1}.

to an average atomic mass dependence as other modes such as $A_g(1)$ are seen to do, with the addition of further splittings occurring, induced by the isotopic disorder. The energy of the most intense $A_g(2)$ component of each isotopically engineered sample does in fact follow a $\bar{m}^{-(1/2)}$ dependence, including the centroid of the 7.3% ^{13}C $A_g(2)$ band which, as can be seen in Fig. 8, is considerably broader than in natural C_{60}, although a ladder of higher energy components is still resolvable. The 56.1% ^{13}C $A_g(2)$ band, shown in the inset of Fig. 8, displays a large broadening from that of natural C_{60}, and no fine structure remains.

It is clear that an explanation of the $A_g(2)$ mode dependence on the isotopic composition of the crystal will require an interplay between isotopic and solid state effects which is presently not well understood. Energy shifts and splittings of the vibrational modes of an isolated C_{60} molecule have been predicted[28,29] to arise from isotopic disorder. A strictly molecular treatment cannot, however, account for the shifting of the strongest crystalline $^{12}C_{60}$ component which occurs as mass substitutions are made in a fraction of the molecules of the solid. Conversely, a ''virtual crystal approximation'' in which the solid is to be modeled by a crystal made up of identical atoms of average mass $\bar{m}$ cannot account for the splittings which occur with increasing ^{13}C content, and the softening of some components but not others within the same band.

In contrast to the complex behavior of the $A_g(2)$ band, several of the lower energy intramolecular modes are well described within a ''virtual crystal approximation.'' Shown in Fig. 9 are the $H_g(1)$ and $A_g(1)$ bands for the isotopically engineered C_{60} crystals described in the preceding paragraphs. As the ^{13}C concentration is increased, the modes merely soften by $\bar{m}^{-(1/2)}$, where $\bar{m}$ is the average isotope mass. The increasing amount of isotopic disorder in the higher ^{13}C content crystals does lead to increased linewidths, with a pronounced lower energy asymmetry appearing in the 56.1% ^{13}C material.

It has been shown herein that the bulk of the splittings displayed in Fig. 2 are not due to mass defects, and so must arise from a crystal field splitting of the molecular modes. While a symmetry analysis of the ordered, low temperature phase of solid C_{60} will predict crystal field splittings for all

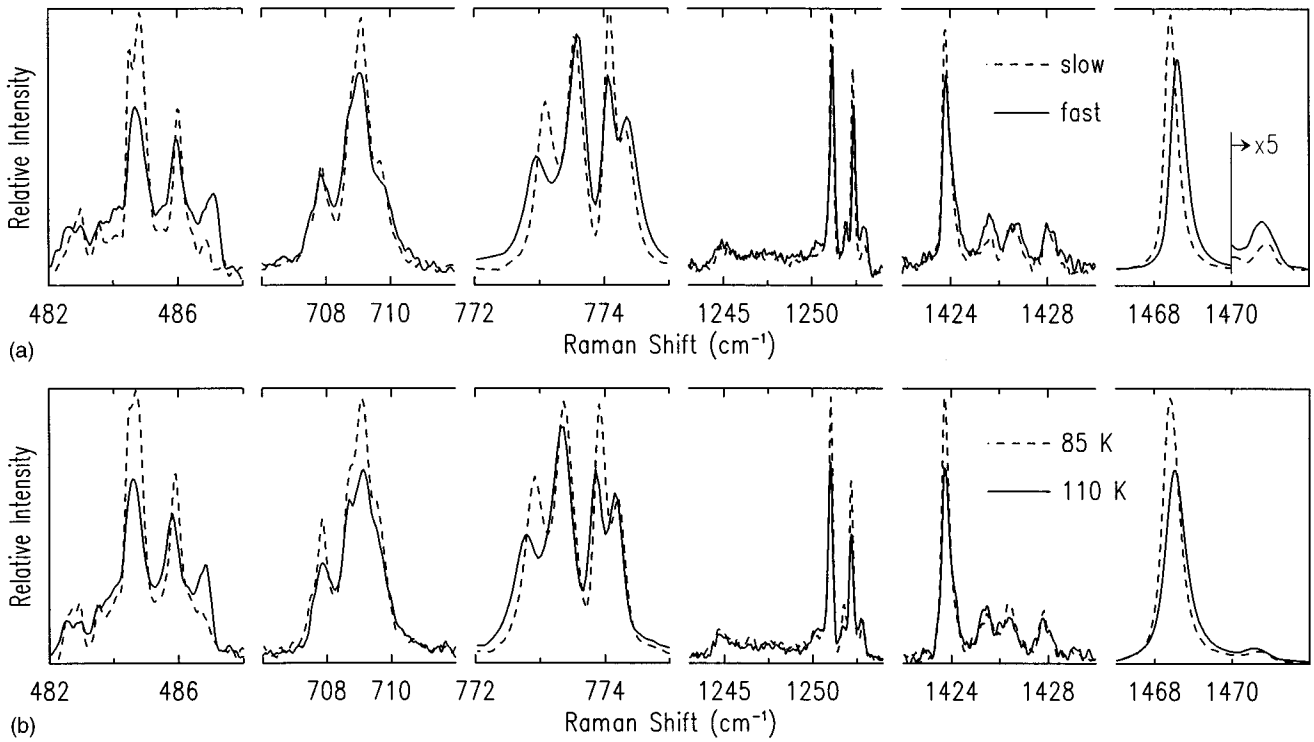

FIG. 10. (a) $G_g(1)$, $H_g(3)$, $H_g(4)$, $H_g(6)$, $H_g(7)$, and $A_g(2)$ fine structure of crystalline $^{12}C_{60}$ at $T=2$ K as a function of the rate of cooling into the glassy state. The ''fast'' quench spectra have been scaled to the ''slow'' quench spectra by matching the intensities of the $A_g(1)$ mode which has no fine structure in either natural or $^{12}C_{60}$. The weak, higher energy peak in the $A_g(2)$ spectra have been multiplied by a factor of 5 for clarity. See text for an explanation of fast and slow quench. (b) The modes displayed in (a) are shown for the samples equilibrated at $T=85$ and 110 K.

of the Raman-active vibrational modes,[3] an additional component due to intrinsic crystal defects in the form of merohedral disorder was recently shown to play a dominant role for several of the intramolecular phonons.[17] The perturbations associated with having an unavoidable fraction of C_{60} molecules misoriented in the low temperature crystal can in fact be seen to influence a majority of the Raman fine structure, as illustrated in Fig. 10. The dependence of the phonon bands on the merohedral disorder can be observed in a straightforward manner by varying the amount of disorder present at low temperature through sample quenching. In Fig. 10(a), six intramolecular vibrational bands of crystalline $^{12}C_{60}$ at 2 K are shown for two different cooling rates. The slow quench corresponded to cooling the crystals from room temperature to 85 K over the span of 12 h, and then cooling to 2 K, while the fast quench involved dropping the crystals directly from room temperature into superfluid helium (crystals were also quenched rapidly from ~220 to 2 K; no difference was found between these and samples quenched directly from room temperature in which the crystals first pass through the fcc-sc ordering transition). A faster quench leads to a higher percentage of misoriented molecules at low temperature (<85 K), since the sample will have passed through the ''glassy'' transition at a higher temperature. All of the modes in Fig. 10(a) show a dependence upon the amount of residual disorder present at low temperature, to varying degrees. Very pronounced changes in the relative intensities of $G_g(1)$, $H_g(4)$, and $A_g(2)$ fine structure are evident, while the changes in $H_g(3,6,7)$ are less dramatic. Although not shown in Fig. 10(a), the relative intensities of components within the $H_g(2)$ and $F_{2g}(1)$ bands also display a minor dependence upon the quench rate.

Since the concentration of misoriented molecules increases as the sample is warmed above the glassy transition, the relative intensity changes which occur in the Raman fine structure with quench rate should simply mirror the temperature evolution of the slowly-quenched sample above the glassy transition. This is clearly seen in Fig. 10(b), which shows the Raman fine structure at 85 and 110 K. The components within a band which grow in intensity relative to others as the temperature is raised are also those which show an increased relative intensity with the fast quench. The comparison between the quench rate and temperature evolution data is complicated by the overall decrease of the Raman intensity of all the modes with increasing temperature. The decrease in integrated intensity stems possibly from a reduced transparency of the material with increasing temperature.

We have previously shown that the merohedral disorder of the crystal leads directly to the $G_g(1)$ and $A_g(2)$ fine structure (of $^{12}C_{60}$ crystals) by studying in detail the temperature dependence of the modes.[17] The relative intensities of the $G_g(1)$ and $A_g(2)$ components followed an Arrhenius type behavior between 85 and 250 K, with an activation energy of ~12 meV. The 12 meV activation energy coincides with previous determinations of the energy increase of a misoriented molecule.[30,31] An equivalent dependence of the remaining modes shown in Fig. 10 is not seen. While all the

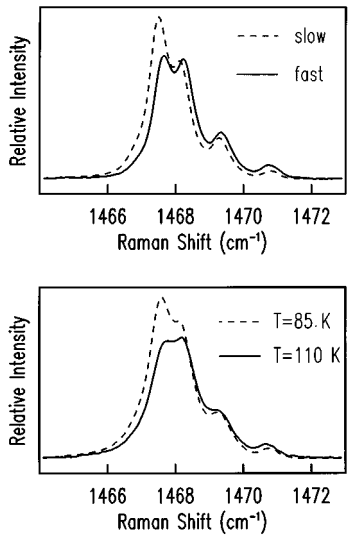

FIG. 11. $A_g(2)$ fine structure of natural crystalline C_{60} at $T=2$ K as a function of the rate of cooling into the glassy state (upper spectra). See text for an explanation of fast and slow quench. Also shown is the $A_g(2)$ mode of natural crystalline C_{60} for samples equilibrated at $T=85$ and 110 K (lower spectra).

modes in Fig. 10 are clearly affected by random orientational defects, delineating this influence from the crystal field of an ordered solid was not possible. Surprisingly, the components of $A_g(2)$ which were activated by the mass defects present in natural C_{60} also displayed an intensity variation with quench rate and temperature. Shown in Fig. 11 is the $A_g(2)$ mode of natural crystalline C_{60} at 2 K for two different quench rates. The intensity variations and energy shifts of the components with increasing quench rate are mirrored in the temperature evolution of the mode, as seen in the bottom portion of Fig. 11, indicating that these changes arise from the merohedral disorder of the low-temperature phase.

Ideally, one would like to study a crystal which is completely in its orientational ground state, but no means of preparing such a sample has yet been discovered. It has been shown that under modest hydrostatic pressure a new orientational phase becomes the ground state of the sc crystal.[32] The new phase is also metastable at zero pressure provided the sample temperature is kept below $\sim$85 K, above which temperature the molecules would reorient to the conventional structure.[18] The amount of residual disorder in the new orientation can be arbitrarily lowered simply by applying higher pressures while the sample is in thermal equilibrium. In the highly ordered state, dramatic simplifications in the intermolecular and intramolecular phonon spectra were seen, particularly in the $G_g(1)$ band. This suggests that equivalent simplifications would be seen in the fine structure of the conventional low temperature phase of crystalline C_{60} if the amount of merohedral disorder could be equivalently reduced.

It is worth noting that the only phonon band whose fine-structure components do not display a dependence on the merohedral disorder of the LT phase is the $H_g(1)$-derived band. The four components of $H_g(1)$ were independent of quench rate, and showed no temperature evolution above the glassy transition, apart from a linewidth broadening and an overall decrease in the integrated Raman intensity. The splittings of $H_g(1)$ can therefore be attributed solely to the crystal field of an ordered solid. This is consistent with the results of a hydrostatic pressure study of crystalline C_{60} (Ref. 18) in which the pressure-induced changes in the molecular orientations altered the fine structure of all the phonons except $H_g(1)$.

Finally, the possibility that portions of the splittings shown in this work stem from more rudimentary defects such as crystal dislocations or impurities can be neglected. None of the phonon fine structure displayed any variation among the large number of crystals which have been produced in our lab over a wide range of conditions. Samples which had been grown in vacuum and then transferred to a cold cryostat without breaking vacuum showed Raman fine structure identical to that of samples which had been handled in air, as did samples subjected to multiple sublimation regrowths versus crystals grown from as-received powder. Nor was any variation in the Raman fine structure encountered with increasing laser irradiance in the near infrared, a phenomenon which is widely reported for visible excitation.[9,14]

CONCLUSION

We have presented high-resolution first-order Raman spectra of isotopically controlled crystalline C_{60}. In isotopically ''pure'' $^{12}C_{60}$ and $^{13}C_{60}$, splittings of nearly all the Raman-active modes are seen. These splittings arise from the crystal field of both the orientationally ordered solid and the small percentage of misoriented molecules present at even the lowest temperatures.

As ^{13}C substitutions were made in crystalline $^{12}C_{60}$, a range of responses was seen in the intramolecular phonon spectrum, from a uniform softening of the lower energy modes along with a disorder-induced asymmetric line broadening, to the very pronounced splittings of $A_g(2)$. This mode-specific effect of the isotopic disorder is presently not well understood, and cannot be accounted for within purely molecular treatments of the isotopic disorder of C_{60} as have been reported to date.

ACKNOWLEDGMENTS

This work was supported by the Natural Sciences and Engineering Research Council of Canada. We are indebted to Cambridge Isotope Labs for assistance in obtaining the ^{12}C and ^{13}C enriched methane gas.

[1] A. Cheng and M. L. Klein, J. Phys. Chem. **95**, 6750 (1991).
[2] T. Yildirim and A. B. Harris, Phys. Rev. B **46**, 7878 (1992).
[3] G. Dresselhaus, M. S. Dresselhaus, and P. C. Eklund, Phys. Rev. B **45**, 6923 (1992).
[4] J. Yu, L. Bi, R. K. Kalia, and P. Vashishta, Phys. Rev. B **49**, 5008 (1994).
[5] E. Burgos, E. Halac, and H. Bonadeo, Phys. Rev. B **49**, 15 544 (1994).
[6] R. Saito, G. Dresselhaus, and M. S. Dresselhaus, Phys. Rev. B **50**, 5680 (1994).
[7] R. L. Cappelleti *et al.*, Phys. Rev. Lett. **66**, 3261 (1991).
[8] L. Pintschovius *et al.*, Phys. Rev. Lett. **69**, 2662 (1992).
[9] P. Zhou *et al.*, Appl. Phys. Lett. **60**, 2871 (1992).
[10] V. N. Denisov, B. N. Mavrin, G. Ruani, R. Zamboni, and C. Taliani, Sov. Phys. JETP **75**, 158 (1992).
[11] P. H. M. van Loosdrecht, P. J. M. van Bentum, M. A. Verheijen, and G. Meijer, Chem. Phys. Lett. **198**, 587 (1992).
[12] P. J. Horoyski and M. L. W. Thewalt, Phys. Rev. B **48**, 11 446 (1993).
[13] M. Matus and H. Kuzmany, Appl. Phys. A **56**, 241 (1993).
[14] Z-.H. Dong *et al.*, Phys. Rev. B **48**, 2862 (1993).
[15] K.-A. Wang, A. M. Rao, P. C. Eklund, M. S. Dresselhaus, and G. Dresselhaus, Phys. Rev. B **48**, 11 375 (1993).
[16] M. C. Martin *et al.*, Phys. Rev. B **51**, 2844 (1995).
[17] P. J. Horoyski, M. L. W. Thewalt, and T. R. Anthony, Phys. Rev. Lett. **74**, 194 (1995).
[18] J. A. Wolk, P. J. Horoyski, and M. L. W. Thewalt, Phys. Rev. Lett. **74**, 3483 (1995).
[19] R. Tycko, G. Dabbagh, R. M. Fleming, R. C. Haddon, A. V. Makhija, and S. M. Zahurak, Phys. Rev. Lett. **67**, 1886 (1991).
[20] R. M. Fleming *et al.*, in *Clusters and Cluster-Assembled Materials*, edited by R. S. Averback, J. Bernholc, and D. L. Nelson, MRS Symposia Proceedings No. 206 (Materials Research Society, Pittsburgh, 1991), p. 691.
[21] P. A. Heiney *et al.*, Phys. Rev. Lett. **66**, 2911 (1991).
[22] P. A. Heiney, J. Phys. Chem. Solids **53**, 1333 (1992), and references therein.
[23] K. C. Hass, M. A. Tamor, T. R. Anthony, and W. F. Banholzer, Phys. Rev. B **44**, 12 046 (1991).
[24] S. Guha *et al.*, Phys. Rev. Lett. **72**, 3359 (1994).
[25] W. Krätschmer, K. Fostiropoulos, and D. R. Huffman, Chem. Phys. Lett. **170**, 167 (1990).
[26] P. J. Horoyski and M. L. W. Thewalt, Appl. Spectrosc. **48**, 843 (1994).
[27] H. D. Fuchs *et al.*, Phys. Rev. B **43**, 4835 (1991).
[28] D. E. Weeks, J. Chem. Phys. **96**, 7380 (1992).
[29] F. Negri *et al.*, Chem. Phys. Lett. **211**, 353 (1993).
[30] R. C. Yu, N. Tea, M. B. Salamon, D. Lorents, and R. Malhotra, Phys. Rev. Lett. **68**, 2050 (1992).
[31] F. Gugenberger *et al.*, Phys. Rev. Lett. **69**, 3774 (1992).
[32] W. I. F. David and R. M. Ibberson, J. Phys. Condens. Matter **5**, 7923 (1993).